AFRL-AFOSR-VA-TR-2018-0371

Sub-cycle optical pulse synthesis and stabilization in next-generation optical frequency combs

Chee Wong
UNIVERSITY OF CALIFORNIA LOS ANGELES

07/20/2018
Final Report

Air Force Research Laboratory
AF Office Of Scientific Research (AFOSR)/ RTB1
Arlington, Virginia 22203
Air Force Materiel Command

REPORT DOCUMENTATION PAGE

Form Approved
OMB No. 0704-0188

1. REPORT DATE *(DD-MM-YYYY)*	2. REPORT TYPE	3. DATES COVERED *(From - To)*
04/27/2018	Final report	03/01/2015-02/28/2018

4. TITLE AND SUBTITLE
Sub-Cycle Optical Pulse Synthesis and Stabilization In Next-Generation Optical Frequency Combs

5a. CONTRACT NUMBER

5b. GRANT NUMBER
FA9550-15-1-0081

5c. PROGRAM ELEMENT NUMBER

6. AUTHOR(S)
Chee Wei Wong

5d. PROJECT NUMBER

5e. TASK NUMBER

5f. WORK UNIT NUMBER

7. PERFORMING ORGANIZATION NAME(S) AND ADDRESS(ES)
University of California Los Angeles

8. PERFORMING ORGANIZATION REPORT NUMBER

9. SPONSORING/MONITORING AGENCY NAME(S) AND ADDRESS(ES)
Air Force Office of Scientific Research

10. SPONSOR/MONITOR'S ACRONYM(S)
AFOSR

11. SPONSOR/MONITOR'S REPORT NUMBER(S)

12. DISTRIBUTION/AVAILABILITY STATEMENT
Distribution A - Approved for Public Release

13. SUPPLEMENTARY NOTES

14. ABSTRACT
The YIP program is productive, with 19 conference contribution, 8 invited talks, and 14 journal publications including at Nature, Nature Photonics, Science Advances, Nature Communications, Phys. Rev. Lett., and Phys. Rev. X. Details of selected works are described in the two annual reports and the final report.

Jinghui Yang, a PhD student working on the project, was one of the Honorable Mentions for the Maiman Student Paper Competition. She was awarded for her work on microresonator Turing pattern and THz generation.

15. SUBJECT TERMS

16. SECURITY CLASSIFICATION OF:			17. LIMITATION OF ABSTRACT	18. NUMBER OF PAGES	19a. NAME OF RESPONSIBLE PERSON
a. REPORT	b. ABSTRACT	c. THIS PAGE			Chee Wei Wong
U	U	U	SAR	10	19b. TELEPHONE NUMBER *(Include area code)* (310) 825-6115

INSTRUCTIONS FOR COMPLETING SF 298

1. REPORT DATE. Full publication date, including day, month, if available. Must cite at least the year and be Year 2000 compliant, e.g. 30-06-1998; xx-06-1998; xx-xx-1998.

2. REPORT TYPE. State the type of report, such as final, technical, interim, memorandum, master's thesis, progress, quarterly, research, special, group study, etc.

3. DATE COVERED. Indicate the time during which the work was performed and the report was written, e.g., Jun 1997 - Jun 1998; 1-10 Jun 1996; May - Nov 1998; Nov 1998.

4. TITLE. Enter title and subtitle with volume number and part number, if applicable. On classified documents, enter the title classification in parentheses.

5a. CONTRACT NUMBER. Enter all contract numbers as they appear in the report, e.g. F33315-86-C-5169.

5b. GRANT NUMBER. Enter all grant numbers as they appear in the report. e.g. AFOSR-82-1234.

5c. PROGRAM ELEMENT NUMBER. Enter all program element numbers as they appear in the report, e.g. 61101A.

5e. TASK NUMBER. Enter all task numbers as they appear in the report, e.g. 05; RF0330201; T4112.

5f. WORK UNIT NUMBER. Enter all work unit numbers as they appear in the report, e.g. 001; AFAPL30480105.

6. AUTHOR(S). Enter name(s) of person(s) responsible for writing the report, performing the research, or credited with the content of the report. The form of entry is the last name, first name, middle initial, and additional qualifiers separated by commas, e.g. Smith, Richard, J, Jr.

7. PERFORMING ORGANIZATION NAME(S) AND ADDRESS(ES). Self-explanatory.

8. PERFORMING ORGANIZATION REPORT NUMBER. Enter all unique alphanumeric report numbers assigned by the performing organization, e.g. BRL-1234; AFWL-TR-85-4017-Vol-21-PT-2.

9. SPONSORING/MONITORING AGENCY NAME(S) AND ADDRESS(ES). Enter the name and address of the organization(s) financially responsible for and monitoring the work.

10. SPONSOR/MONITOR'S ACRONYM(S). Enter, if available, e.g. BRL, ARDEC, NADC.

11. SPONSOR/MONITOR'S REPORT NUMBER(S). Enter report number as assigned by the sponsoring/ monitoring agency, if available, e.g. BRL-TR-829; -215.

12. DISTRIBUTION/AVAILABILITY STATEMENT. Use agency-mandated availability statements to indicate the public availability or distribution limitations of the report. If additional limitations/ restrictions or special markings are indicated, follow agency authorization procedures, e.g. RD/FRD, PROPIN, ITAR, etc. Include copyright information.

13. SUPPLEMENTARY NOTES. Enter information not included elsewhere such as: prepared in cooperation with; translation of; report supersedes; old edition number, etc.

14. ABSTRACT. A brief (approximately 200 words) factual summary of the most significant information.

15. SUBJECT TERMS. Key words or phrases identifying major concepts in the report.

16. SECURITY CLASSIFICATION. Enter security classification in accordance with security classification regulations, e.g. U, C, S, etc. If this form contains classified information, stamp classification level on the top and bottom of this page.

17. LIMITATION OF ABSTRACT. This block must be completed to assign a distribution limitation to the abstract. Enter UU (Unclassified Unlimited) or SAR (Same as Report). An entry in this block is necessary if the abstract is to be limited.

Sub-cycle optical pulse synthesis and stabilization in next-generation optical frequency combs

AFOSR FA9550-15-1-0081: final report

Figure 1 shows the overall layout map of the 12" Si_3N_4 wafer fabricated under the support of this grant. The wafer consists of more than 100 devices for novel Kerr comb synthesizers. The tapeout designs include six different types of devices: 1, coupled-ring geometry to investigate comb mode-locking dynamics; 2, cascaded-ring configuration to study microresonator chaos; 3, microring with slotted waveguide for broadband dispersion tuning; 4, microring with varying waveguide width for generation of dispersion managed soliton; 5, microring with waveguide geometry optimized for Kerr comb induced by cross-phase modulation instability; 6, dual ring system to investigate Kerr comb's intrinsic timing jitter and evaluate the feasibilities of on-chip optical pulse synthesizer and dual comb spectroscopy.

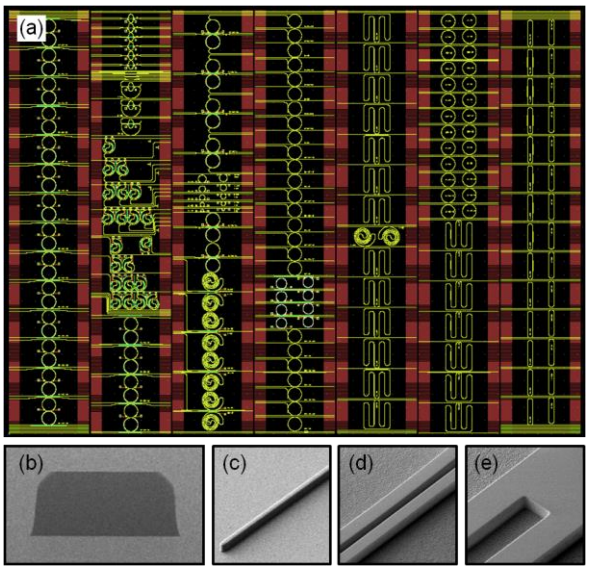

Figure 1. (a) Overall layout map of the 12" Si_3N_4 wafer, consisting of more than 100 difference devices. (b) TEM image of the waveguide, measuring a sidewall angle of 97°. (c)-(e) SEM images of adiabatic mode converter, evanescence wave coupler, and multimode interference coupler.

Baseline measurement of the fabricated waveguide confirms a sidewall angle of 97°, a propagation loss of 0.2 dB/cm, and a smallest feature of 200 nm. Fiber-to-fiber coupling loss of 5 dB and loaded quality factor of 1,300,000 with critical coupling are achieved in these newly developed Si_3N_4 microresonators. The bandwidth of the multimode interference coupler, for coherent multispectral synthesis, is characterized to be larger than 300 nm.

1. Smooth and flat Kerr frequency comb generation by higher order mode suppression

We report a novel design of Si_3N_4 microresonator such that single mode operation, high quality factor, and anomalous dispersion are attained simultaneously. The microresonator is consisted of uniform single mode waveguides in the semi-circle region, to eliminate bending induced mode coupling, and adiabatically tapered waveguides in the straight region, to ensure selective excitation of the fundamental mode. The intrinsic Q of the microresonator is 1.36×10^6, 1.6 times larger than that of a single mode microresonator with a uniform waveguide cross-section. More importantly, the group velocity dispersion of the novel microresonator remains to be anomalous at -50 fs^2/mm. We demonstrate, with this novel microresonator, phase-locked Kerr frequency combs can be

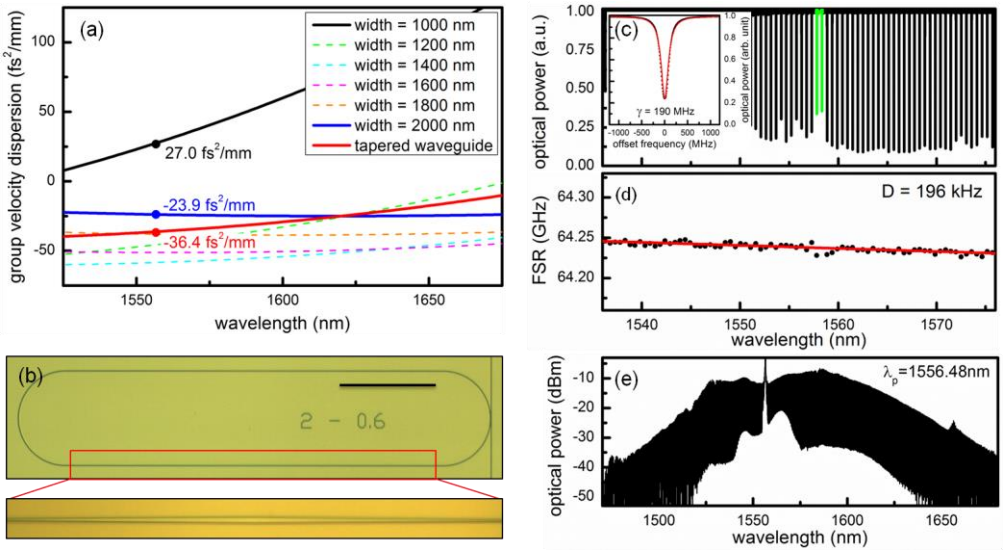

Figure 2. (a) Calculated group velocity dispersion of the uniform waveguides with different widths and the tapered waveguide, taking into account both the waveguide dimensions and the material dispersion. (b) An optical micrograph of the designed single-mode microresonator. The waveguide in the semi-circle regions has a uniform width of 1 μm, supporting only the fundamental modes. On the other hand, the 800 μm long straight waveguide has a tapered width from 1 μm at the end to 2 μm at the middle of the waveguide. The total cavity length is 2.2 mm. Scale bar: 200 μm. (c) Cold cavity transmission of the designed single-mode microresonator. Higher order modes are not observed in the microresonator, but the weak TE and TM coupling around 1558 nm results in a 10% reduction in the cavity loading (green lines). Inset: resonance at 1556 nm is undercoupled with a loaded Q of 1,000,000. (d) Wavelength dependence of the free spectral range, measuring a non-equidistance of the modes, $D = -\frac{\beta_2 c \omega_{FSR}^2}{n}$, of 196 kHz. The extracted group velocity dispersion is anomalous at -50 fs^2/mm. The slight dispersion disruption around 1558 nm is negligible in the Kerr frequency comb formation, evidenced by the smooth spectral shape shown in (e). Such smooth and flat comb spectra can be generated by pumping at any resonances in the optical C-band.

generated by pumping at any resonances in the optical C-band. The spectra spanning more than 20 THz (full width at -20 dB) are smooth without periodic amplitude modulations.

Publication: S.-W. Huang, H. Liu, J. Yang, *et al.*, "Smooth and flat phase-locked Kerr frequency comb generation by higher order mode suppression", *Scientific Reports* **6**, 26255 (2016).

2. A stabilized chip-scale optical frequency comb with a relative uncertainty of 2.7×10^{-16}

We report the first fully stabilized CMOS-compatible chip-scale optical frequency comb with a frequency relative uncertainty down to 2.7×10^{-16}. The silicon nitride spiral resonator is designed and fabricated to generate a Kerr microcomb, at 18 GHz native spacing and spanning more than 8 THz over more than 400 comb lines. Its single-sideband phase noise reaches the instrument limited floor of -130 dBc/Hz at 1 MHz offset. To stabilize the comb's first degree-of-freedom, the external cavity diode laser (ECDL) is phase-locked to an optical reference, here a mode of a stabilized fiber laser frequency comb, and then amplified to 2 W to pump the Si_3N_4 microresonator. The residual deviation of the pump frequency over 1000 seconds is instrument-limited at 1 mHz. To stabilize the comb's second degree-of-freedom, the comb spacing is monitored by sending the comb to a

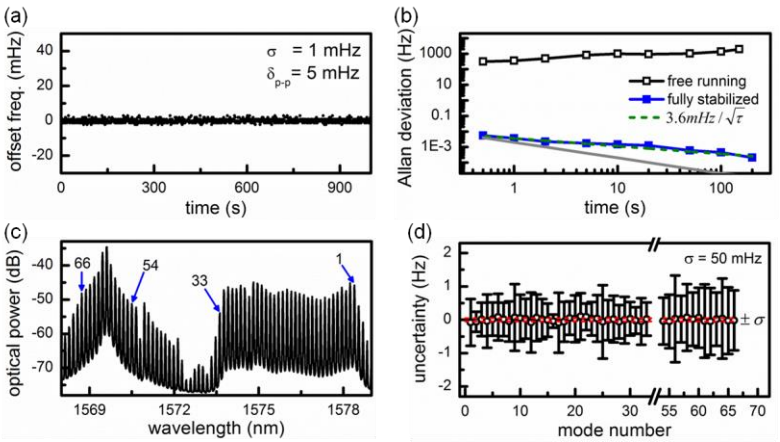

Figure 3. (a) Frequency counting of the stabilized beat note with a gate time of 1 s. The standard deviation over 1000 seconds is 1 mHz, instrument-limited by the stability of the frequency counter. (b) Allan deviation of the free-running (black open squares) and fully stabilized (blue closed squares) comb spacing. The fully stabilized comb spacing shows a consistent trend of 3.6 mHz/$\sqrt{\tau}$ (green dashed line) when the gate time is in the range from 0.5 s to 200 s. The gray line denotes the counter-limited Allan deviation. (c) To quantify the accuracy of the stabilized chip-scale optical frequency comb, each of the comb lines from 1578.4 to 1573.6 nm (m=1 to m=33) and from 1570.5 to 1568.7 nm (m=54 to m=66) is mixed with the fiber laser frequency comb and the beat frequency is counted with a gate time of 1 s. (d) Counting results on the optical frequencies of 46 comb lines. The centroid of the comb frequencies stray from the ideal with a 190 mHz peak-to-peak deviation and a 50 mHz standard deviation.

high-speed photodetector (3 dB bandwidth more than 15 GHz) and downmixing the electronic signal to the baseband with a local oscillator at 18 GHz. A fiber electro-optic modulator controls the pump power and stabilizes the comb spacing. Active stabilization on the comb spacing improves the RF stability by six orders of magnitude, reaching residual instrument-limited close-to-carrier (10 Hz) phase noise of -70 dBc/Hz and Allan deviation of 3.6 mHz/$\sqrt{\tau}$. In the optical frequency, forty-six lines of the Kerr microcomb subset are selected and compared against the current benchmark fiber laser frequency comb and the frequency relative uncertainty of the stabilized Kerr microcomb is demonstrated down to 50 mHz, or 2.7×10^{-16} when referenced to the 188 THz optical carrier. The reported system is a promising compact platform for coherent Raman spectroscopy, optical clockwork, coherent communications, arbitrary waveform generation, and astrophysical spectrography.

Publication: S.-W. Huang, J. Yang, M. Yu, *et al.*, "A broadband chip-scale optical frequency synthesizer at 2.7×10^{-16} relative uncertainty", *Science Advances* **2**, e1501489 (2016).

3. High-*Q* photonic reference for Kerr comb stabilization

Leveraging the Kerr comb stabilization demonstration described in Sec. 2, we go beyond and develop a miniaturized optical reference based on the high *Q* whispering gallery mode (WGM) crystalline microresonator technology. Collaborating with OEwaves, we attain an MgF_2 WGM microresonator with a quality factor of 2.4×10^9. Furthermore, the microresonator is sandwiched by a laminating Zerodur structure to reduce its sensitivity to thermal expansion noise by a factor of three. The MgF_2 WGM microresonator is used as the optical reference to stabilize the pump frequency, the first degree-of-freedom of the Kerr comb, through the Pound–Drever–Hall (PDH) technique. We modulate the pump frequency to find a cavity resonance by applying a triangle

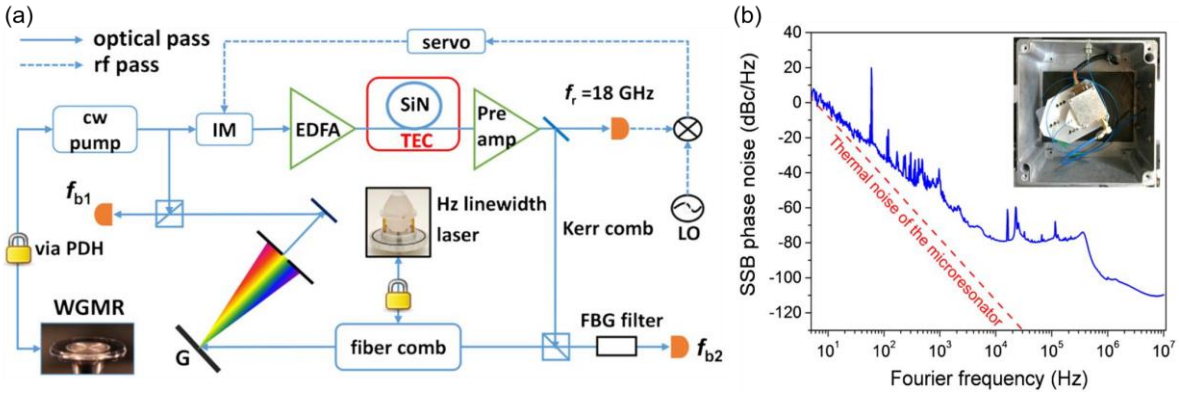

Figure 3. (a) Experimental setup. Both the pump and the Kerr comb stabilities are measured by beating them against a fiber laser comb stabilized independently to a 1 Hz linewidth reference laser. IM, intensity modulator; G, reflection grating; LO, local oscillator; TEC, thermo-electric cooler; FBG, fiber Bragg grating. (b) SSB phase noise of the pump laser stabilized to the WGM microresonator reference (blue solid line) with the thermorefractive noise limit of the WGM microresonator shown in the red dashed line. Inset: the packaged WGM microresonator in an aluminum box. TEC, photodetector, and coupling optics are integrated in a small footprint (40 mm×40 mm×15 mm).

modulation voltage to the ECDL current modulation knob that is eventually used to stabilize the laser to the high-*Q* photonic reference with a bandwidth of 1 MHz. The PDH error signal is optimized by controlling the modulation depth and frequency on the phase modulator and coupling power into the resonator for the best stabilization performance. Figure 3b shows the single sideband (SSB) phase noise of the stabilized pump laser by beating it against a fiber laser frequency comb independently stabilized to a 1 Hz linewidth reference laser. The phase noise of the stabilized pump is close to the thermorefractive noise limit near the carrier frequency regime, achieving a level of -2.5 dBc/Hz at 10 Hz offset frequency. Noise peaks from the 60 Hz electric power line noise and acoustic noise can be further reduced by devising a better enclosure for acoustic and thermal isolation. The second degree-of-freedom of the Kerr comb, the comb spacing, is stabilized using the same method described in Sec. 2. The PID control bandwidth is 125 kHz. The Kerr comb stability reaches 2.3×10^{-11} at 1 s averaging time. The fractional instability increases with longer averaging times, implying that the long-term stability of the WGM optical reference is limited by the uncompensated thermo-mechanical noise. The green triangle shows the fractional instability of the stabilized Kerr comb and it is improved by more than two orders of magnitude at 1 s averaging time, compared with the free-running comb (black squares) to 4.9×10^{-11}. Above the 1 s averaging time, it follows the fractional instability of the pump.

Publication: J. Lim, S.-W. Huang, A. Kumar, *et al.*, "Stabilized chip-scale Kerr frequency comb via a high-Q reference photonic microresonator", *Opt. Lett.* **41**, 3706 (2016).

4. Globally stable Turing pattern formation for coherent high-power THz radiation

We report the spontaneous formation of globally stable Turing patterns in chip-scale nonlinear oscillators, uniquely enabled by local mode hybridization. We devise a novel scheme to circumvent Turing pattern destabilization that fundamentally limits the available Turing pattern energy and achievable power conversion efficiency. We attain globally stable Turing pattern formation in chip-scale nonlinear oscillators with significantly enlarged parameter space, achieving a record-high power-conversion efficiency of 45%, more than a factor of 5 enhancement, and an elevated peak-to-valley contrast of 100. The terahertz pattern is step-wise tunable across 430 GHz, and symmetry breaking of the Turing roll spectra is also observed. We interrogate the commensurate and coherent nature of the spontaneous dissipative structure with ultrafast optical intensity autocorrelation, microwave spectral noise analysis, and heterodyne beating against a benchmark fiber frequency comb. The Turing pattern sideband frequency non-uniformity is measured down to 1 part in 1.5×10^{15}, with a short-term (200 ms sweep time) linewidth of 9 kHz and a long-term (over 20 minutes) drift of 160 kHz. We transfer the Turing pattern coherence to the terahertz (THz) radiation with a plasmonic ErAs:InGaAs photomixer, generating up to 600 μW

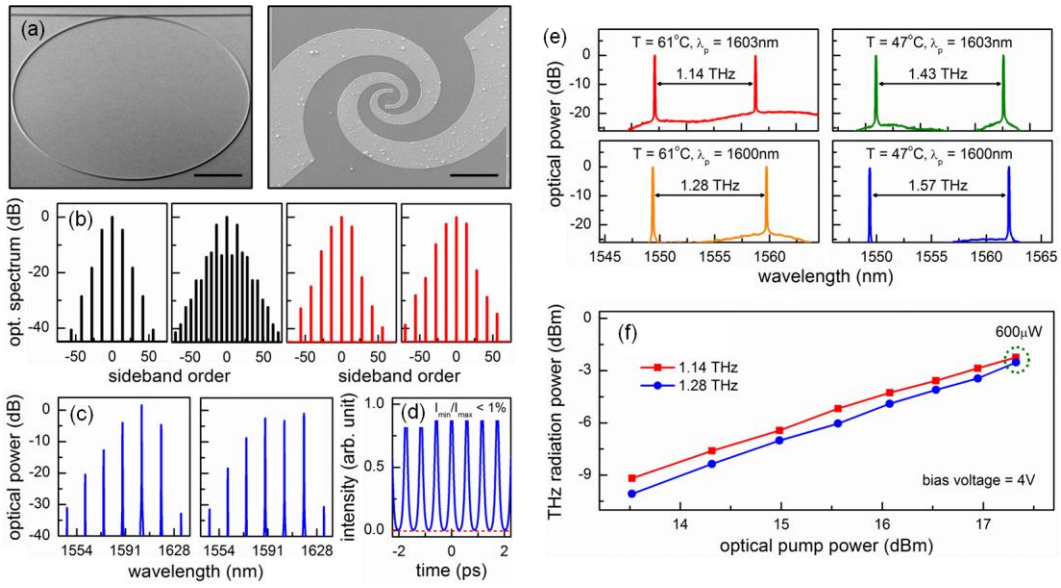

Figure 4. (a) SEM images of the microring and the plasmonic photomixer. Scale bar: 100 μm. (b) Lugiato-Lefever modeling of the spontaneous Turing pattern formation. In the anomalous dispersion regime (black curves), a spontaneous growth of symmetric Turing roll is observed. As the wavelength was tuned closer to resonance, sub-comb started to emerge and destabilize the Turing pattern. On the other hand, growth of Turing roll is prohibited in the normal dispersion regime unless local dispersion disruption by mode hybridization is introduced (red curves). Here sub-comb growth and transition into chaos are forbidden, with a clear broken spectral symmetry. (c) Example Turing roll spectra at different pump laser-cavity detuning. Close to the resonance, a strong pump depletion and highly efficient Turing roll generation up to 45% power conversion is observed in the measurement. (d) Measured intensity profile of the sub-picosecond Turing roll, showing a quasi-sinusoidal oscillation with a more than 100 contrast. (e) Turing roll repetition rate, and hence the generated THz frequency, can be tuned by changing the pump wavelength and the resonator temperature. (f) THz radiation power as a function of optical pump power. Power conversion efficiency of 1.1 % can be obtained with an optical pump power of 54 mW.

THz radiation power at high 1.1% optical-to-THz power conversion at room temperature, with applications in astrophysics, atmospheric sensing, and precision spectroscopy.

Publication: S.-W. Huang, J. Yang, S.-H. Yang, *et al.*, "Globally stable microresonator Turing pattern formation for coherent high-power THz radiation on-chip", *Phys. Rev. X* **7**, 041002 (2017).

5. New operation regime of Kerr frequency comb

We propose and demonstrate a new type of Kerr frequency comb where the momentum conservation law is fulfilled by azimuthal modulation of the waveguide dispersion. We consider the case in which the azimuthal mode numbers of the signal and idler are not symmetrically located with respect to the pump mode. We show, both analytically and experimentally, that Kerr frequency comb can still be generated given that an azimuthal modulation of the cavity parameters is introduced to provide an additional wavevector for quasi-phase matching (QPM).

Our use of a Si_3N_4 planar microresonator has the advantage of straightforward dispersion management by the design of waveguide geometry, opening up the possibility of implementing the QPM concept via azimuthal GVD modulation. In a good agreement with the theoretical analysis, we demonstrate a multispectral Kerr frequency comb covering important fiber-optic communication bands. Comb coherence and absence of a sub-comb offset are confirmed by continuous-wave heterodyne beat note and amplitude noise spectra measurements. Different from the traditional Kerr frequency comb formation dynamics where the growth of secondary comb lines is associated with high-noise incoherent chaos, here the coherence of the QPM Kerr frequency comb surprisingly remains without destabilization into chaos. The rigorous physical understanding of such a phenomenon requires further investigation.

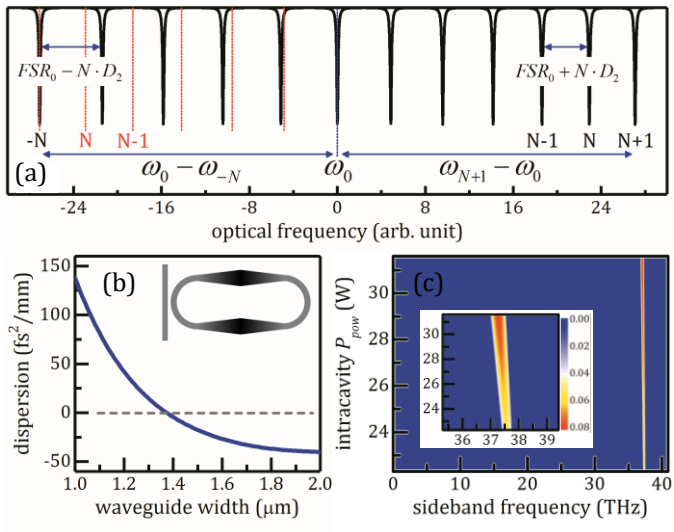

Figure 5. (a) Principle of the QPM Kerr frequency comb generation, assuming that the azimuthal mode numbers of the signal and idler are not symmetrically located with respect to the pump mode. While the energy conservation law of $\omega_{N+1} + \omega_{-N} - 2\cdot\omega_0 = 0$ can be satisfied, the momentum conservation law is always violated unless an azimuthal modulation of the cavity parameters is introduced to provide an additional wavevector for the QPM condition. The red dashed lines show the resonance frequencies that are mirrors of the signal modes with respect to the pump mode. (b) COMSOL-modeled GVD of the Si_3N_4 waveguide with respect to the waveguide width. Inset: Schematic of our dispersion-modulated single-mode Si_3N_4 microresonator. (c) Analytic gain of Faraday ripples as a function of the sideband frequency and intra-cavity pump power. Inset: Zoom-in map of the roundtrip gain coefficient, showing the gain peak of Faraday ripples at approximately 37.5 THz.

The concept and principle can be applied to other types of microresonators and expand the scope of Kerr frequency comb. The reported

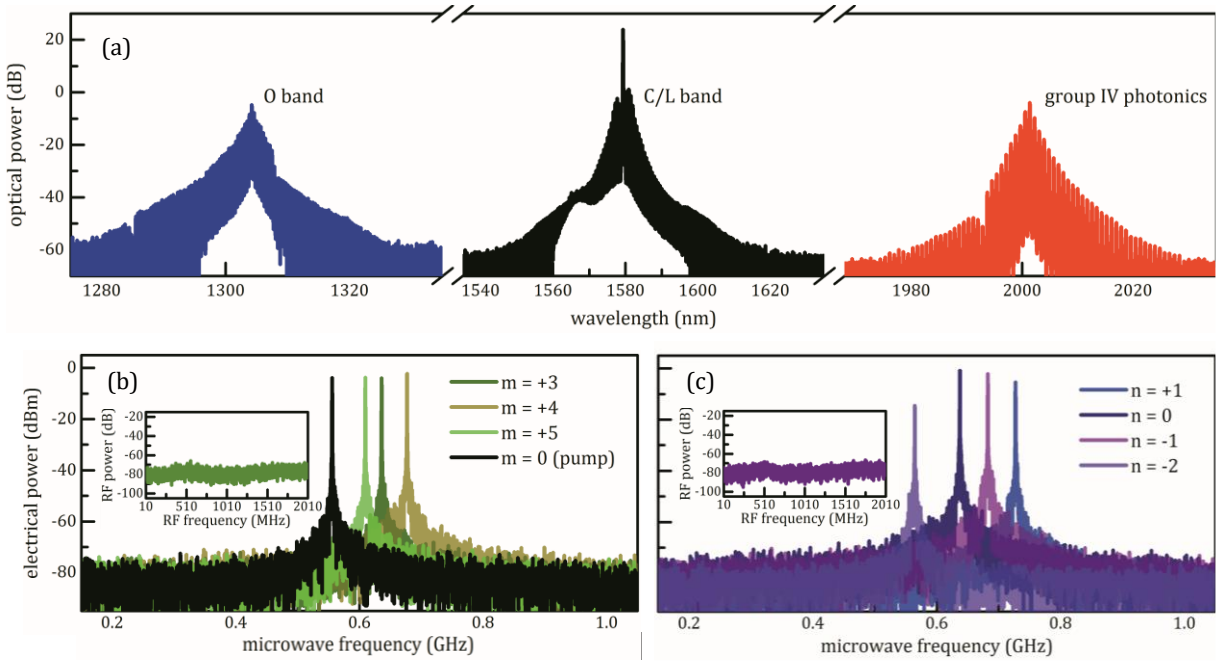

Figure 6. (a) The QPM multispectral Kerr frequency comb covers important fiber-optic communication bands, including the emerging 2-μm channel that is compatible with group IV photonics. Both the O band and the C/L band combs span more than 8 THz above the OSA noise floor, while the 2 μm comb spans a narrower 4 THz owing to the aberration in the NIR coupling optics. The overall bandwidth spans more than 2/3 of an octave. (b) Heterodyne beat notes and RF amplitude noise spectrum (inset) of the C/L band Kerr frequency comb. m = 0 corresponds to the pump mode at 1580 nm. (c) Heterodyne beat notes and RF amplitude noise spectrum (inset) of the O band Kerr frequency comb. n = 0 corresponds to the comb line at 1304 nm.

QPM multispectral Kerr frequency comb is a promising platform for broadband optical frequency synthesizers and high-capacity coherent communication. Higher order QPM is theoretically predicted, but we have not observed it experimentally. Further investigation can lead to the demonstration of higher order QPM Kerr frequency comb that will find applications in quantum optics and precision sensing.

Publication: S.-W. Huang, A. K. Vinod, J. Yang, *et al.*, "Quasi-phase-matched multispectral Kerr frequency comb", *Opt. Lett.* **42**, 2110 (2017).

6. Panoramic-reconstruction temporal imaging

Studying the dynamics of dissipative Kerr solitons is of particular interest because of its potential applications in low-phase noise photonic oscillator, broadband optical frequency synthesizer, miniaturized optical clockwork, and coherent terabit communications. While the Kerr nonlinearity and soliton generation benefit greatly from the microresonator's ultrahigh quality factor (Q), the ultrahigh Q also renders its formation and transition dynamics to be slowly evolved at a time scale much longer than the cavity roundtrip time. Similarly, an optical metrology system that combines the feats of fine temporal resolution and long measurement window is desired in study of optical turbulence and laminar-turbulent transition in fiber lasers, which leads to better

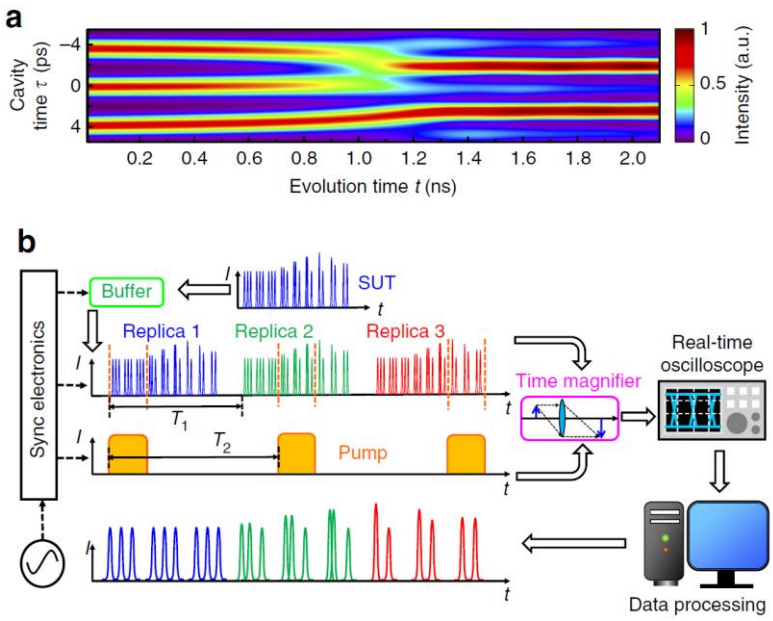

Figure 7. Working principle of the PARTI system. (a) Slowly evolved dissipative Kerr soliton dynamics in an ultrahigh-*Q* microresonator, obtained by numerically solving the Lugiato–Lefever equation. The orders-of-magnitude difference in the timescale between the cavity time and the evolution time poses an experimental challenge to capture the comprehensive picture of the dynamics. (b) The schematic representation of the PARTI system. The optical buffer generates multiple replicas (represented by blue, green and red, respectively) of the SUT and the subsequent time magnifier captures different portions of the SUT waveform on each replica. After data processing on the system output, the original long SUT waveform can be reconstructed through waveform stitching.

understanding of coherence breakup in lasers and laser operation in far-from-equilibrium regimes. To capture comprehensive portraits of these processes, as well as many other transient phenomena in nonlinear optical dynamics, a temporal imaging system with a time-bandwidth product (TBWP) much greater than 1,000 is necessary.

Inspired by the space-time duality and the wisdom of stitching multiple mosaic microscopic images to achieve larger field of view in the spatial domain, we devise a panoramic-reconstruction temporal imaging (PARTI) system to scale up temporal record length without sacrificing the resolution. As a proof-of-concept demonstration, the PARTI system is applied to study the dynamic waveforms of slowly-evolved dissipative Kerr solitons in an ultrahigh-*Q* microresonator. Two 1.5-ns-long comprehensive evolution portraits are reconstructed with 740-fs resolution and dissipative Kerr soliton transition dynamics in which multiple soliton state evolves into stable singlet soliton state are meticulously depicted for the first time (Fig. 8).

Publication: B. Li, S.-W. Huang*, Y. Li, *et al.*, "Panoramic-reconstruction temporal imaging for seamless measurements of slowly-evolved femtosecond pulse dynamics", *Nature Commun.* **8**, 61 (2017).

7. Gate-tunable frequency combs in graphene-nitride microresonators

The intracavity dispersion is one of the most critical parameter that defines the Kerr frequency comb formation dynamics in monolithic ultrahigh-*Q* microresonators. Despite its significance, until now the cavity dispersion is unfortunately an immutable property predefined only by the waveguide design. Furthermore, since light is tightly confined in the wavelength-scale waveguide,

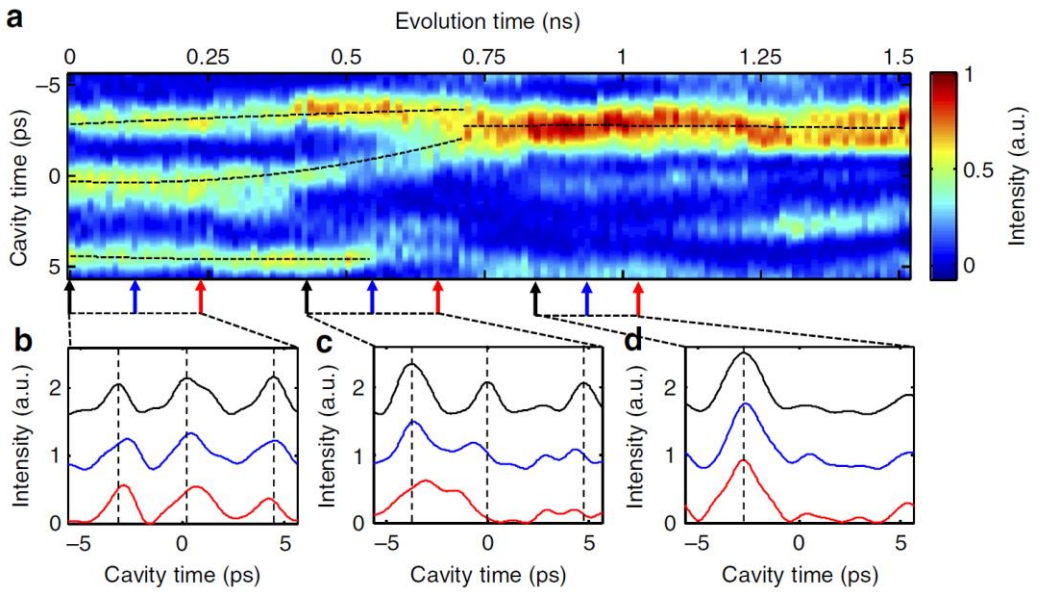

Figure 8. Dissipative Kerr soliton dynamics measured by the PARTI system. (a) An example 2D evolution portrait, depicting soliton fusion dynamics and transition from a triplet soliton state to a singlet soliton state. (b)–(d) Measured waveforms at different evolution time slices in each stage, illustrating stable triplet solitons at the beginning stage (b), soliton fusion at the middle stage (c) and stable singlet soliton in the final stage (d).

its dispersion is inevitable prone to intrinsic nanometer-scale fabrication errors which result in device-to-device deviations from the designed dispersion values.

Here, by using a graphene-based dual-layer transistor with ionic liquid as the gate electric, we tune the Fermi level of graphene up to 0.65 eV, incorporated on an optical ring cavity. Our graphene-nitride microresonator implementation enables a microresonator with widely gate-tunable group velocity dispersion (GVD), from anomalous to normal region (-62 fs^2/mm to 9 fs^2/mm). Consequently, we achieve the dynamic generation and operation of Kerr frequency combs for the first time.

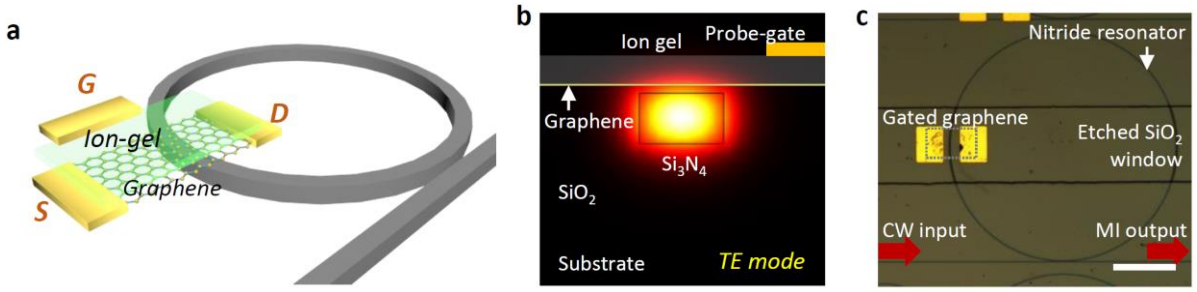

Figure 9. Conceptual design and implementation of the gate-tunable graphene-nitride heterogeneous microcavity. (a) Schematic architecture of the GMR. A graphene/ion-gel heterostructure is incorporated in the nitride microresonator. (b) E-field distribution of the graphene-nitride heterogeneous waveguide, with a Si_3N_4 cross section of 1.2 × 0.8 μm^2. The distance between the Si_3N_4 waveguide and the graphene layer is 100 nm. Graphene and the top gate probe is separated by 1 μm with the interlayer ion-gel capacitor. In this structure, TE mode is applied. (c) Optical micrographs show the bus waveguide (red arrows), ring resonator and Au/Ti metallized patterns. An etched window is designed to ensure both the graphene-light interaction and a reduced propagation loss. Here the graphene covered area is marked by the grey dashed box. Scale bar: 100 μm.

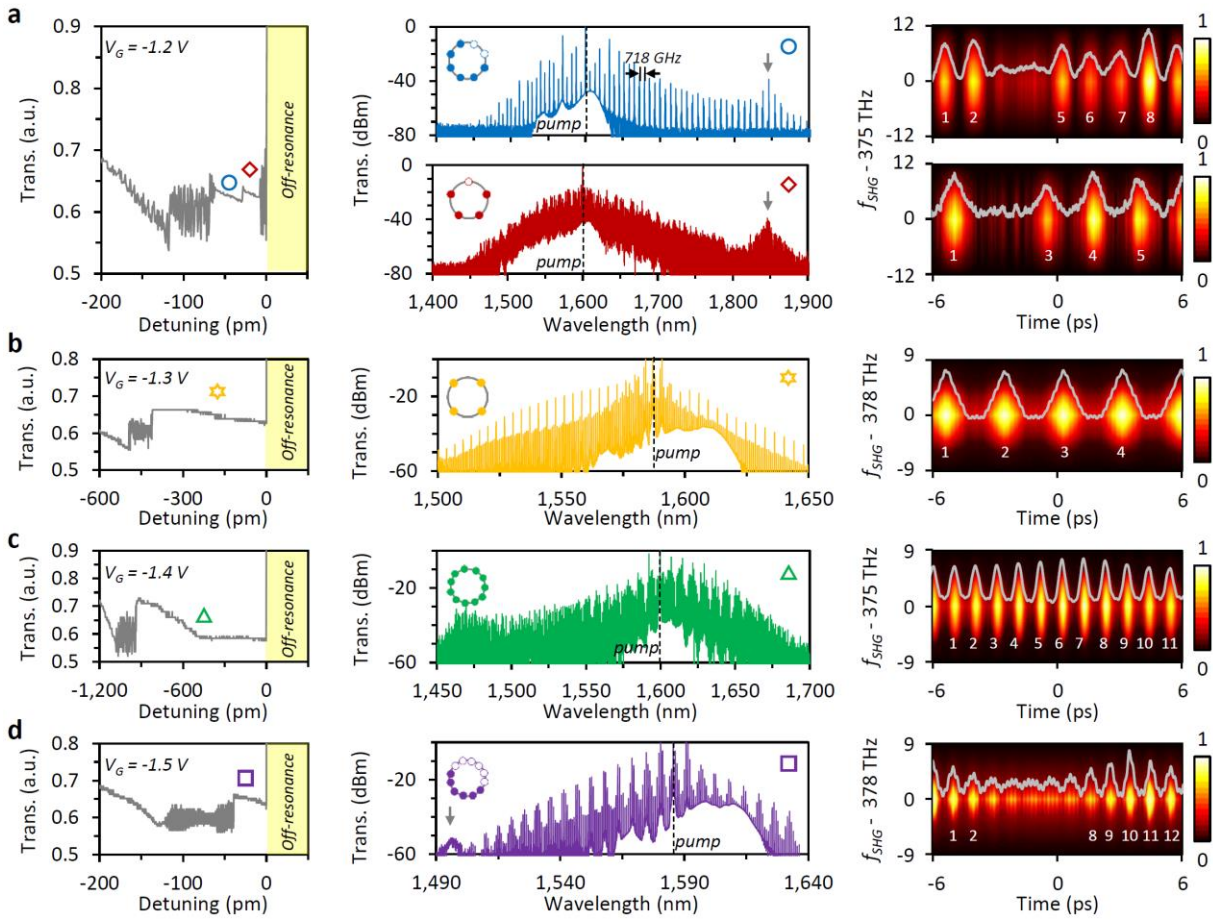

Figure 10. Soliton crystals of the gated graphene-nitride microresonator. (a) and (d), Soliton state with crystal-like defects including the single-soliton defect in panel (a). (c) and (d), Periodic soliton crystal states with equally spaced soliton pulses. Panels (a) to (d) are achieved with gate voltage V_G tuned from -1.2 V to -1.5 V respectively. Left panels: measured intensity transmission, illustrating the characteristic steps associated with soliton formation. Middle panels: corresponding optical spectra measurements. The pump locations are marked by black dashed line and the Cherenkov radiation peaks are marked by grey arrows. Right panels: frequency-resolved second-harmonic autocorrelation maps of the soliton pulses. Here the grey curves show the corresponding second-harmonic intensity autocorrelation traces.

We uncover the formation of tunable primary comb lines, coherent Kerr frequency combs, and controllable soliton states with adjustable Cherenkov radiation, – all in a single microcavity. We further demonstrate the controlled transitions from periodic soliton crystals to crystals with defects, mapped by our ultrafast second-harmonic optical autocorrelation. This heterogeneous graphene-nitride microcavity provides a new fundamental platform for the understanding of dynamical frequency combs and ultrafast optics at the interface of single atomic layer nanoscience and ultrafast optoelectronics.

Publication: B. Yao, S.-W. Huang*, Y. Liu, *et al.*, "Gate-tunable frequency combs in graphene-nitride microresonators", *Nature* accepted (2018).